Current Biology 23, 1242–1250, July 8, 2013 ©2013 Elsevier Ltd All rights reserved http://dx.doi.org/10.1016/j.cub.2013.05.037

Report

Metabolic Regulation of Cellular Plasticity in the Pancreas

Nikolay Ninov,[1,2,*] Daniel Hesselson,[1,3,4] Philipp Gut,[1] Amy Zhou,[1] Kevin Fidelin,[1,5] and Didier Y.R. Stainier[1,2,*]
[1]Department of Biochemistry and Biophysics, Programs in Developmental and Stem Cell Biology, Genetics and Human Genetics, the Diabetes Center, Institute for Regeneration Medicine and Liver Center, University of California, San Francisco, 1550 4th Street, San Francisco, CA 94158, USA
[2]Department of Developmental Genetics, Max Planck Institute for Heart and Lung Research, Ludwigstrasse 43, 61231 Bad Nauheim, Germany
[3]Diabetes and Obesity Program, Garvan Institute of Medical Research, Sydney, New South Wales 2010, Australia
[4]St. Vincent's Clinical School, University of New South Wales, Sydney, New South Wales 2052, Australia
[5]Centre de Recherche de l'Institut du Cerveau et de la Moelle épinière, Université Pierre et Marie Curie, 75651 Paris, France

Summary

Obese individuals exhibit an increase in pancreatic β cell mass; conversely, scarce nutrition during pregnancy has been linked to β cell insufficiency in the offspring [reviewed in 1, 2]. These phenomena are thought to be mediated mainly through effects on β cell proliferation, given that a nutrient-sensitive β cell progenitor population in the pancreas has not been identified. Here, we employed the fluorescent ubiquitination-based cell-cycle indicator system to investigate β cell replication in real time and found that high nutrient concentrations induce rapid β cell proliferation. Importantly, we found that high nutrient concentrations also stimulate β cell differentiation from progenitors in the intrapancreatic duct (IPD). Furthermore, using a new zebrafish line where β cells are constitutively ablated, we show that β cell loss and high nutrient intake synergistically activate these progenitors. At the cellular level, this activation process causes ductal cell reorganization as it stimulates their proliferation and differentiation. Notably, we link the nutrient-dependent activation of these progenitors to a downregulation of Notch signaling specifically within the IPD. Furthermore, we show that the nutrient sensor mechanistic target of rapamycin (mTOR) is required for endocrine differentiation from the IPD under physiological conditions as well as in the diabetic state. Thus, this study reveals critical insights into how cells modulate their plasticity in response to metabolic cues and identifies nutrient-sensitive progenitors in the mature pancreas.

Results and Discussion

β Cell Mass Increases in Response to Increased Feeding

There is a tight correlation between nutrient intake and β cell mass in nondiabetic obese individuals (reviewed in [1, 3]) and experimental models of overnutrition [4, 5]. Whether nutritional cues impinge on the renewal and differentiation of β cell progenitors remains to be investigated. In mice, β cell progenitors are found in the embryonic pancreatic ducts [6–8]. Analogously, in zebrafish, β cells arise from epithelial cells lining the intrapancreatic duct (IPD) [9, 10]. A unique advantage of the zebrafish model is the ability to visualize these ductal progenitors in vivo [9, 11]. To explore the nutritional control of β cell progenitors, we analyzed β cell mass dynamics during two major metabolic transitions. First, by 5 days postfertilization (dpf) (Figure 1A), larvae deplete nutrients stored in the yolk and transition into a feeding state. Second, between 15–16 dpf, larvae are switched to a high-calorie diet and grow rapidly until late juvenile stages (45 dpf) (Figure 1B) [12]. To characterize β cell mass responses during these transitions, we examined *Tg(TP1:H2BmCherry);Tg(ins:GFP)* animals. *Tg(TP1:H2BmCherry)* drives H2BmCherry expression in Notch-responsive cells (NRCs) in the IPD [9]. Given that H2BmCherry has a long half-life, this transgenic combination allows the in vivo monitoring of NRCs to β cell differentiation (Figure 1C). This differentiation forms secondary islets (SIs) along the IPD [9, 11]. Intriguingly, we observed a dramatic increase in SI number and principal islet (PI) size after switching to a high-calorie diet at 15 dpf (Figures 1D–1G). The new SIs were vascularized, and individual β cells appeared to establish contact with blood vessels (Figures S1A and S1B available online), suggesting that they contribute to the functional β cell mass.

β Cells Transition from Quiescence to Proliferation in Response to Nutrients

This rapid β cell mass increase after switching to a high-calorie diet suggests that increased nutrient intake stimulates β cell proliferation and/or differentiation. To determine the role of proliferation, we developed transgenics using the fluorescent ubiquitination-based cell-cycle indicator (FUCCI) system for real-time quantification of proliferation [13, 14]. We placed (zFucci-G1) and (zFucci-S/G2/M) under the *insulin* promoter for β-cell-specific expression (Figure S1C). At 4.5 dpf, *Tg(ins:*zFucci-G1*)* expression labeled the majority of β cells in the PI, whereas *Tg(ins:*zFucci-S/G2/M*)* expression labeled rare cells (Figures 1H and S1C). To assess this system's dynamics, we performed live imaging at 4.5 dpf. *Tg(ins:*zFucci-S/G2/M*)* labeling disappeared shortly after mitosis (Figure 1H), indicating precise labeling of proliferating β cells. To validate this system further, we performed 5-ethynyl-2′-deoxyuridine (EdU) analyses at 30 dpf. Strikingly, the vast majority of *Tg(ins:*zFucci-S/G2/M*)* single-positive cells (90% ± 12%, n = 9 animals) were also EdU^+, whereas a minor fraction of *Tg(ins:*zFucci-S/G2/M*);Tg(ins:*zFucci-G1*)* double-positive cells had incorporated low levels of EdU (Figures S1D–S1F). These double-positive cells are most likely in a very early stage of S phase. For precision, we only scored *Tg(ins:*zFucci-S/G2/M*)* single-positive cells as proliferating β cells. Notably, after the switch to a high-calorie diet at 15 dpf, β cell proliferation increased throughout the day, peaking 10–12 hr after the first feeding (Figures 1I–1J). Furthermore, β cells in SIs also exhibited high proliferation (Figure S1G). To test whether this β cell proliferation was stimulated by nutrients, we deprived animals of food for 28 hr. Fasting dramatically reduced the number of proliferating β cells (2.5 ± 2.2 cells per PI, n = 14 islets)

*Correspondence: nikolay.ninov@mpi-bn.mpg.de (N.N.), didier.stainier@mpi-bn.mpg.de (D.Y.R.S.)

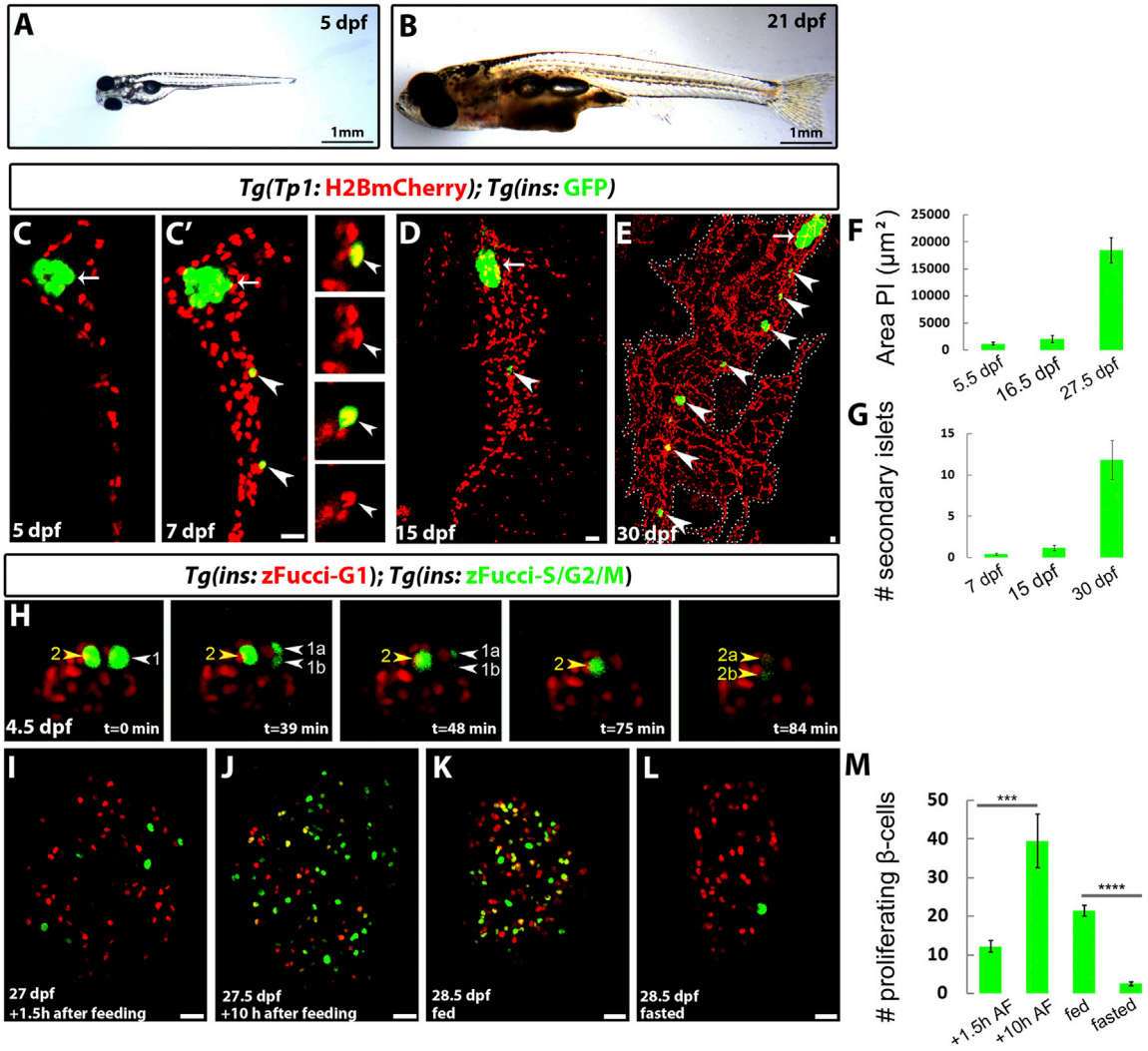

Figure 1. β Cells Transition from Quiescence to Proliferation in Response to Nutrients

(A and B) Wild-type (WT) animals imaged at 5 (A) and 21 (B) dpf showing the dramatic growth that takes place in the feeding animal.

(C–E) *Tg(TP1:H2BmCherry);Tg(ins:GFP)* larvae were examined with confocal imaging. *Tg(TP1:H2BmCherry)* drives the expression of H2BmCherry in NRCs in the IPD, and *Tg(ins:GFP)* labels β cells. Arrows point to the principal islet (PI). Arrowheads point to secondary islets (SI).

(C and C') The larva was imaged live at 5 (C) and at 7 (C') dpf. At 7 dpf, two new β cells (arrowheads) had formed posterior to the PI. These cells derived from NRCs, given that they were also *Tg(Tp1bglob*:H2BmCherry)$^{+}$. The insets show single planes with separated channels. At 7 dpf, 0.45 (±0.6, n = 21 larvae) β cells containing SIs per larva were present posterior to the PI.

(D) At 15 dpf, the number β cells containing SIs per larva was 1.2 (±1.3, n = 22 larvae).

(E) At 30 dpf, there was a dramatic increase in the number of β cells, which clustered in multiple SIs (11.8 ± 5.7 SIs per animal, n = 6 animals). The pancreas is outlined by a dashed line.

(F) Quantification of the PI's area at 5.5, 16.5 and 27.5 dpf, showing a dramatic increase in its size between 16.5 and 27.5 dpf (n = 6 animals at 5.5 and 16.5 dpf; 5 animals at 27.5 dpf).

(G) Quantification of the number of *Tg(ins*:GFP)$^{+}$ SIs at 7, 15, and 30 dpf showing a dramatic increase between 15–30 dpf (n = 22 animals at 7 and 15 dpf; 6 animals at 30 dpf).

(H) Live imaging of a *Tg(ins:zFucci-G1);Tg(ins:zFucci-S/G2/M)* larva at 4.5 dpf. A projection of the stack is shown. At t = 0 min, two *Tg(ins*:zFucci-S/G2/M)$^{+}$ β cells (arrowheads) were present in the PI. Both cells (1 and 2) divided during the course of the imaging, resulting in the downregulation and the subsequent loss of *Tg(ins*:zFucci-S/G2/M*)* expression in their daughter cells (1a and 1b and 2a and 2b, respectively).

(I–L) *Tg(ins:zFucci-G1);Tg(ins:zFucci-S/G2/M)* animals were used to examine the effects of nutrients on β cell proliferation; the images show single confocal planes through the PI.

(I–J) Animals from the same clutch were fixed at 1.5 (I) or 10 hr (J) after feeding (AF) starting at 27 dpf. Several β cells (12.2 ± 4.3 β cells, n = 9 animals) were proliferating 1.5 hr AF.

(J) The number of proliferating β cells increased at 10 hr AF (39 ± 23 β cells, n = 11 animals, ***$p < 0.005$).

(K) The animals were fed regularly and examined at 28.5 dpf (12 hr AF). Numerous β cells in the PI were proliferating (21.4 ± 4 β cells, n = 7 animals).

(L) Animals from the same clutch as in (K) were deprived of food for 28 hr and examined at 28.5 dpf. The number of proliferating β cells in the PI was dramatically reduced (2.5 ± 2.2 β cells, n = 14 animals, ****$p < 0.0001$).

(M) Quantification of the average number of proliferating β cells in the PI for the experiments shown in (I)–(L).

(A), (B), and (H) are lateral views, anterior to the left and dorsal to the top; (C) and (D) are lateral views, anterior to the top and dorsal to the left; and (E) and (I)–(L) are dorsal views, anterior to the top. Error bars represent SEM, and scale bars represent 20 µm.

See also Figure S1.

(Figures 1L and 1M) in comparison to the number of controls (21.4 ± 4 cells, n = 7 islets) (Figures 1K and 1M). The effects of fasting were reversible, given that β cells re-entered the cell cycle upon refeeding (data not shown). This nutrient-driven β cell proliferation was also observed at earlier time points after switching to a high-calorie diet (Figures S1H and S1I). Thus, β cell mass expansion is dynamically regulated by nutritional intake.

Nutrients Enhance β Cell Differentiation from the IPD

Proliferation alone does not explain the increase in the number of SIs, and, thus, nutrients may also induce β cell differentiation. First, we analyzed whether β cells in an SI originate from the differentiation of a single, rare IPD cell followed by clonal expansion or whether they derive from multiple IPD cells. This question is important because, in mice, IPD cells appear to lose progenitor potential around birth [6–8]. A tamoxifen-inducible Cre recombinase was placed under the control of the Notch-responsive element (TP1) *Tg(TP1:CreERT2)*. Using the ubiquitous reporter *Tg(ubi:Switch)* [15] and 2F11 immunofluorescence, which marks IPD cells [16], we observed that 4-hydroxytamoxifen (4-OHT) treatment at 14 dpf mosaically labeled IPD cells by 17 dpf (Figures 2A, S2A, and S2B). Next, we used *Tg(TP1:CreERT2)* in combination with the *Tg(insulin:Switch)* reporter [17]. In this combination, β cells that originate from IPD cells containing *Tg(TP1:*CreERT2*)* activity exhibit H2BGFP expression instead of mCherry expression. In a single-progenitor scenario and under limiting 4-OHT treatments, each SI would be composed of H2BGFP$^+$ or mCherry$^+$ cells. In a multiple-progenitor scenario, SIs would be mosaic, containing both H2BGFP$^+$ and mCherry$^+$ cells (Figure 2B). Thus, we treated larvae with 4-OHT at 16 dpf and analyzed pancreata at 35–40 dpf. The lineage-traced cells contributed to mosaic SIs (Figure 2C), containing up to three discrete H2BGFP$^+$ cells per SI (Figure 2D), which indicated that multiple IPD cells contribute to an individual SI. We did not detect H2BGFP$^+$ cells in the SIs 2 days after the 4-OHT pulse (Figure S2C), indicating that H2BGFP$^+$ cells originated from neogenesis rather than from pre-existing β cells that had retained CreERT2 activity. Moreover, adding 4-OHT before SIs form (2.5 dpf) also led to mosaic SI labeling at 32 dpf (Figure S2D), supporting the multiclonality of β cells in SIs, which was consistent with the polyclonality of mouse [18–20] and human [21] islets. Within the PI, we observed groups of H2BGFP$^+$ cells (8 ± 3.4 cells per group, n = 7 groups) (Figure 2E), suggesting that individual NRCs differentiated into β cells and then underwent several amplification rounds. We also detected H2BGFP$^+$ cells in proximity to SIs (Figure 2F). Subsequent analyses using *Tg(TP1:H2BmCherry);Tg(ins:GFP)* revealed newly differentiated β cells approaching an SI via directed migration (Figure 2G). To directly test the involvement of nutrients in β cell differentiation, we compared the number of SIs in animals that were switched to a high-calorie diet versus siblings maintained on a low-calorie diet between 15–20 dpf (Figures 2H and 2I). The restricted diet significantly reduced the formation of new SIs (Figure 2J), indicating that high nutrient levels induce β cell differentiation.

IPD Cells Exhibit a Strong Regenerative Response to β Cell Ablation under Feeding

Whether IPD cells can increase their endocrine differentiation rate after a selective β cell loss remains unknown, as does the metabolic control of such a response. To address these questions, we employed a transgenic system in which β cells express the cell-lethal diphtheria toxin α (DTA) chain [22] under the control of the *insulin* promoter, leading to complete ablation without a bystander effect (D.H., unpublished data). Conditional β cell ablation is achieved by *Tg(ins:*Cre*)*-mediated excision of the blue fluorescent protein (BFP) cassette from the floxed *ins:loxp:BFPloxp:DTA* transgene. In the absence of β cells, the PI core was occupied by α cells (Figures S3A and S3B).

We examined β-cell-ablated animals under fasting metabolism (5–6 dpf) [23] and during feeding (15–21 dpf). At 5 dpf, they were viable and exhibited a slight body-length reduction in comparison to WT animals (WT = 3.7 ± 0.11 mm; β-cell-ablated animals = 3.5 ± 0.09 mm, n = 12 animals per group, $p < 0.0001$). To monitor IPD endocrine lineage differentiation, we used *Tg(TP1:H2BmCherry)* in combination with the pan-endocrine marker *Tg(neuroD:*GFP*)*. Quantification of the number of *Tg(neuroD:*GFP*)*$^+$ SIs revealed no differences in endocrine differentiation in β-cell-ablated animals by 6.5 dpf (Figures 3A, 3B, and 3E).

Under external nutrition (16.5 dpf), β-cell-ablated animals feed actively, as indicated by the presence of food in their intestinal tract (Figure S3C), and exhibit similar lethality (1 out of 20) to that of controls (2 out of 20). However, they exhibit a significant growth retardation (Figures S3C and S3D), suggesting that insulin stimulates growth in zebrafish as it does in humans [24, 25]. In addition, β-cell-ablated animals exhibited higher free glucose levels (9.85 ± 2.2 pmol/μg, n = 6 animals) in comparison to their unablated siblings (3.64 ± 0.31 pmol/μg, n = 3 animals, $p < 0.001$). Strikingly, by 15.5 and 16.5 dpf, β-cell-ablated animals presented excessive numbers of ectopic *Tg(neuroD:*GFP*)*$^+$ cells in the pancreatic tail (Figures 3C, 3D, 3F, and S3E–S3G). A majority of *Tg(neuroD:*GFP*)*$^+$ cells also exhibited *Tg(TP1:*H2BmCherry*)* expression, indicating differentiation from pancreatic NRCs (Figure S3G). By 21 dpf, the ectopic *Tg(neuroD:*GFP*)*$^+$ cells gave rise to hormone-producing endocrine cells, including glucagon$^+$ cells (Figures S3H and S3I). In addition, at 16.5 dpf, we observed discrete β cells that had clearly differentiated from NRCs (Figures 3H and S3G). This enhanced endocrine differentiation was accompanied by cell clustering and reduced branching of the IPD (Figure 3H) as well as a loss of duct cell markers, including 2F11 immunofluorescence (Figures 3G and 3H). Using EdU analysis at 20.5 dpf, we also found an increase in NRC replication from 8.8% (±2.86%, n = 9 animals) in wild-type (WT) animals to 22.9% (±5.45%, n = 9 animals) in β-cell-ablated animals exhibiting IPD clustering (Figures S3J–S3L). To test whether feeding at earlier stages could stimulate endocrine differentiation, we counted SIs after feeding from 5–6.5 dpf. This short feeding did not significantly increase the number of SIs in β-cell-ablated animals (1.4 ± 1.13 SIs, n = 13 animals) in comparison to WT animals (1.28 ± 1.05 SIs, n = 21 animals) ($p > 0.5$). Thus, only under sustained feeding does the lack of β cells trigger a strong regenerative response in β cell progenitors, stimulating their proliferation and endocrine lineage differentiation.

IPD Cells Lose Notch Signaling in the Absence of β Cells

The IPD phenotypes in β-cell-ablated animals, including endocrine cell differentiation and increased proliferation, resemble those of animals with impaired Notch signaling during early larval stages [9]. Therefore, we examined Notch signaling levels using the previously validated *Tg(TP1:H2BmCherry);Tg(TP1:VenusPEST)* transgenic system [9]. Cells with active Notch signaling are double positive for H2BmCherry and VenusPEST, whereas cells that recently lost Notch

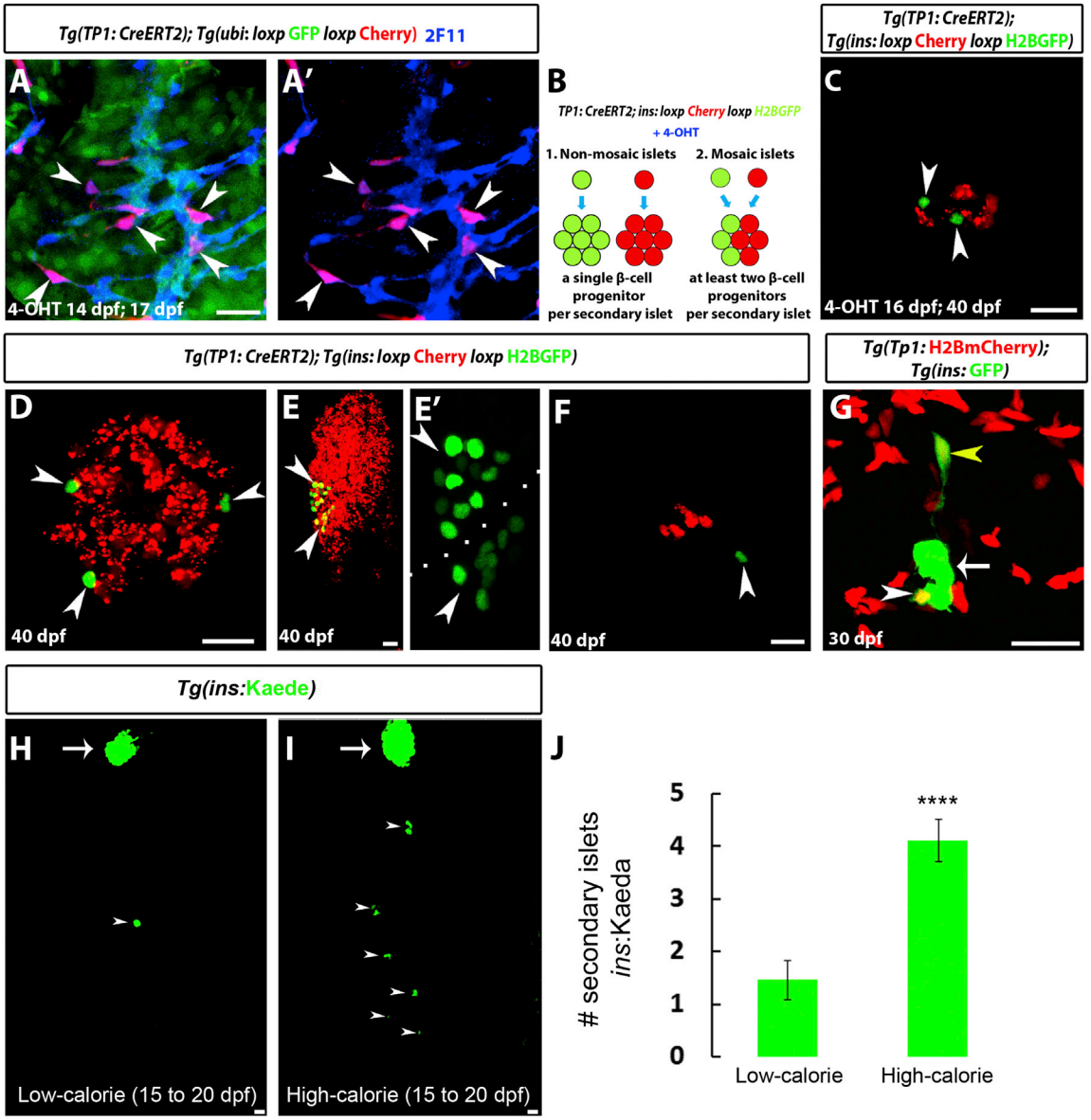

Figure 2. Nutrients Regulate β Cell Differentiation

(A) *Tg(TP1:CreERT2);Tg(ubi3C:loxp-GFP-loxp:mCherry)* larvae were treated with 4-OHT at 14 dpf for 16 hr, fixed at 17 dpf, and stained for 2F11 to mark IPD cells. 4-OHT treatment resulted in the mosaic labeling of individual IPD cells (mCherry$^+$;GFP$^-$ cells) (arrowheads).

(B) Experimental setup for the lineage tracing of β cells from IPD cells. *Tg(insulin:loxP*:mCherry-*STOP:loxP*:H2BGFP)$^+$ β cells that originated from IPD cells with *Tg(TP1*:CreERT2*)* activity exhibit H2BGFP expression instead of mCherry expression. In a single-progenitor scenario (1), each SI would be composed of H2BGFP$^+$ or mCherry$^+$ cells, whereas, in a multiple-progenitor scenario (2), SIs would be mosaic, containing both H2BGFP$^+$ and mCherry$^+$ cells.

(C–F) *Tg(TP1:CreERT2);Tg(insulin:loxP:mCherry-STOP:loxP:H2BGFP)* larvae treated with limiting concentrations of 4-OHT at 16 dpf for 16 hr and analyzed at 40 dpf.

(C) A mosaic SI composed of H2BGFP$^+$ (arrowheads) and mCherry$^+$ β cells.

(D) Three individual H2BGFP$^+$ β cells (arrowheads) located in the periphery of a SI, suggesting that they originated from three different IPD cells.

(E) A PI showing two peripheral H2BGFP$^+$ groups of β cells (arrowheads), indicating several cell cycles after differentiation.

(F) A single H2BGFP$^+$ β cell (arrowhead) in proximity to an SI. Of 20 animals treated with 4-OHT, 15 contained lineage-traced cells, whereas no lineage-traced cells were observed in vehicle-treated controls (n = 7 animals, 80 SIs and 7 PIs).

(G) *Tg(TP1:H2BmCherry);Tg(ins:GFP)* animals were examined at 30 dpf. A projection of several planes shows an SI (arrow). The white arrowhead points to a single β cell in the periphery of the SI. The yellow arrowhead points to a single β cell outside the SI, extending a long cellular process toward it. Both of these β cells exhibit higher levels of *Tg(TP1*:H2BmCherry*)* fluorescence in comparison to the rest of the β cells in the SI, suggesting that they recently differentiated and did not undergo proliferation.

(H and I) *Tg(ins:Kaede)* animals were maintained on a low-calorie diet until 20 dpf (H) or switched to a high-calorie diet (I) from 15 to 20 dpf (see Experimental Procedures). Although there is only a single *Tg(ins*:Kaede*)*$^+$ SI (arrowhead) posterior to the PI (arrow) in (H), multiple SIs (arrowheads) formed in (I).

(J) Quantification of the number of SIs posterior to the PI (n = 17 animals for each group). The high-calorie diet induced the formation of more SIs in comparison to the low-calorie diet (****$p < 0.0001$). Error bars represent SEM, and scale bars represent 20 μm.

See also Figure S2.

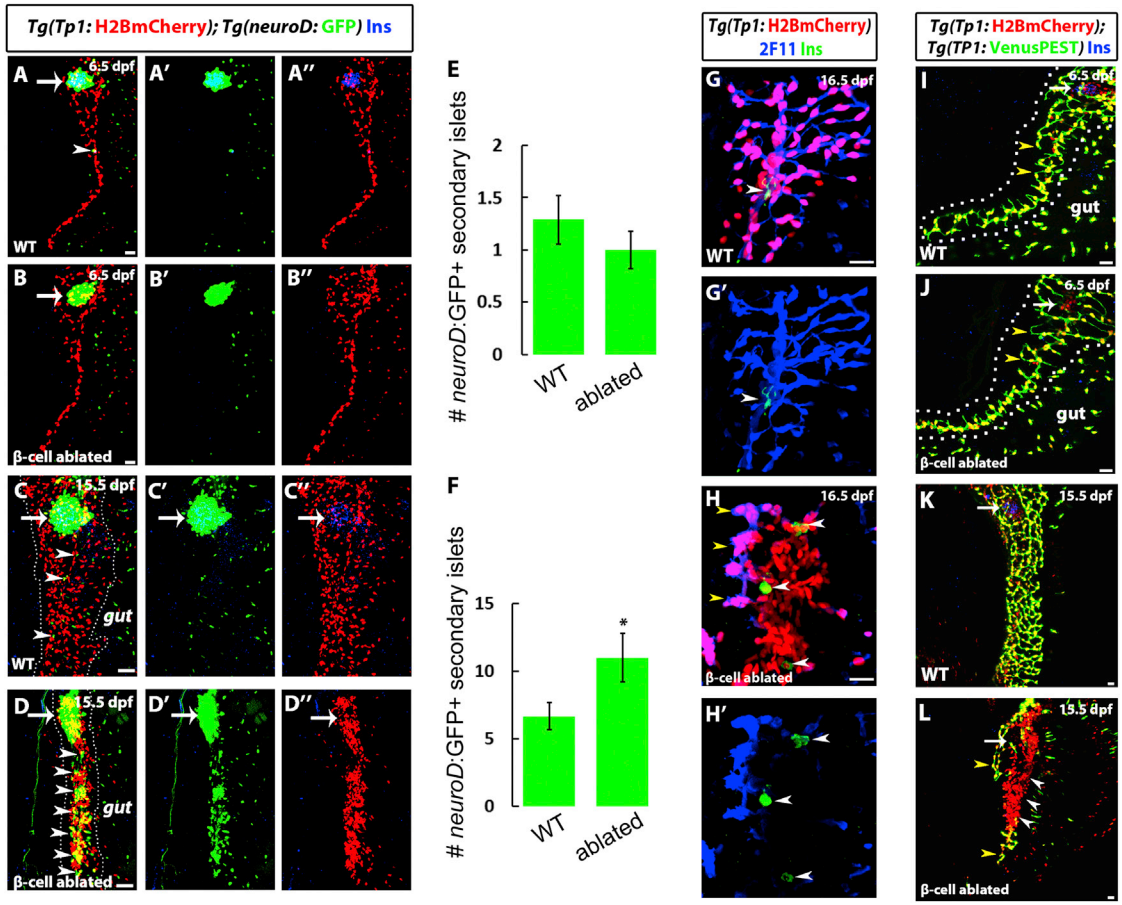

Figure 3. β Cell Ablation Triggers a Regenerative Response in the IPD via Notch Signaling

(A–D) Confocal micrographs of WT and β-cell-ablated animals at the indicated stages. β cells are marked by insulin immunoreactivity (blue). *Tg(TP1*:H2BmCherry*)* expression labels pancreatic NRCs in the IPD, and *Tg(neuroD*:GFP*)* expression marks endocrine cells and their direct precursors. Arrows point to the PI, and arrowheads point to SIs.

(A and B) At 6.5 dpf and in the absence of external nutrition, the β-cell-ablated animals (B) do not exhibit any visible phenotype in the IPD or in the differentiation of NRCs into endocrine cells in comparison to WT animals (A) (n = >30 animals each).

(C and D) Confocal micrographs of WT and β-cell-ablated animals at 15.5 dpf under external nutrition. At this stage, in WT animals (C), the pancreatic NRCs have expanded in numbers, and their nuclei are clearly separated. In contrast, β-cell-ablated animals exhibit a dramatic clustering of the NRCs as well as an increase in the number of SIs composed of *Tg(neuroD*:GFP*)*$^{+}$ cells.

(E) Quantification of the number of SIs for WT (n = 24) and β-cell-ablated (n = 33) animals at 6.5 dpf.

(F) Quantification of the number of SIs for WT (n = 12) and β-cell-ablated (n = 34) animals at 16.5 dpf. Overall, β-cell-ablated animals exhibit a significant increase in the number of SIs (*p = 0.014) in comparison to WT animals.

(G and H) Confocal micrographs of the pancreatic tails of WT (G) and β-cell-ablated animals (H) at 16.5 dpf. β cells are marked by insulin immunoreactivity (green). 2F11 immunoreactivity (blue) marks IPD cells. Whereas, in WT animals, the vast majority of *Tg(TP1*:H2BmCherry*)*$^{+}$ NRCs exhibit 2F11 immunoreactivity and form part of the ductal network, in β-cell-ablated animals, a large proportion of the *Tg(TP1*:H2BmCherry*)*$^{+}$ NRCs have lost 2F11 immunoreactivity as well as ductal organization. Some of these NRCs exhibit insulin immunoreactivity (white arrowheads), indicating an attempted β cell regeneration. Only a few of the *Tg(TP1*:H2BmCherry*)*$^{+}$ cells maintain high 2F11 immunoreactivity (yellow arrowheads).

(I–L) *Tg(TP1:VenusPEST)*, which expresses a fluorescent protein with a short half-life under a Notch-responsive element (TP1), was used to determine the levels of Notch signaling in WT and β-cell-ablated animals at the indicated stages. Arrows point to the PI.

(I and J) At 6.5 dpf, in both WT (I) and β-cell-ablated (J) animals, the IPD cells maintain active Notch signaling and are double positive for *Tg(TP1*:H2BmCherry) and *Tg(TP1*:VenusPEST*)* expression. Note that, in both cases, the IPD cells exhibit branching morphogenesis (yellow arrowheads).

(K and L) At 15.5 dpf, in contrast to WT animals (K) where a majority of IPD cells maintain active Notch signaling, β-cell-ablated animals (L) exhibit a strong reduction in, and even a loss of, Notch signaling in the IPD, as indicated by the presence of numerous *Tg(TP1*:H2BmCherry*)*$^{+}$ but *Tg(TP1*:VenusPEST*)*$^{-}$ cells (white arrowheads). Only some cells with active Notch signaling are present (yellow arrowheads).

All panels show lateral views, anterior to the top and dorsal to the left. Error bars represent SEM, and scale bars represent 20 μm.

See also Figure S3.

signaling lack VenusPEST because of its short half-life. At 6.5 dpf, a majority of IPD cells in WT animals exhibit active Notch signaling (Figure 3I). Similarly, under fasting conditions at 6.5 dpf, the IPD cells in β-cell-ablated animals exhibit active Notch signaling (Figure 3J), which is consistent with a lack of response of NRCs to β cell ablation in the absence of feeding. In contrast, at 15.5 dpf, β-cell-ablated, fed animals exhibited a strong downregulation of Notch signaling in the IPD (Figures 3K and 3L). This downregulation was IPD specific, given that other tissues, including the intrahepatic duct and brain, did not downregulate *Tg(TP1:*VenusPEST*)* expression (Figures S3M and S3N) (data not shown). Furthermore, we examined

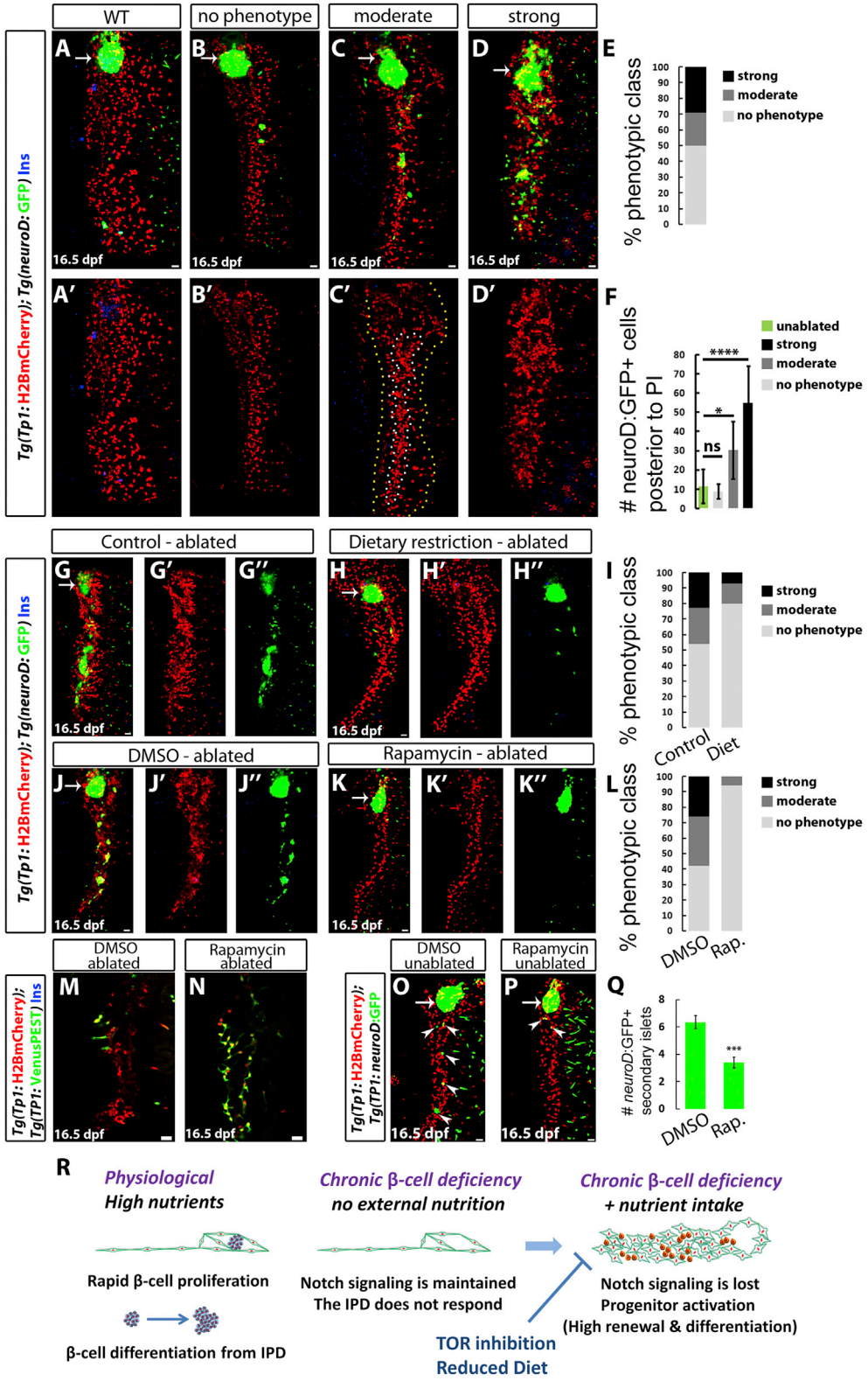

Figure 4. High Nutrient Intake and TOR Signaling Are Required for the Activation of the Regenerative Response of IPD Cells

(A–D) WT (A) and β-cell-ablated (B–D) animals at 16.5 dpf. The phenotypes of β-cell-ablated animals fall into several classes based on the degree of IPD disorganization and the extent of endocrine differentiation.

(B) No phenotype; lack of IPD cell clustering and no increase in ectopic *Tg(neuroD*:GFP)$^{+}$ cells posterior to the PI in comparison to WT animals (quantified in F).

(C) Moderate phenotype; only some *Tg(TP1*:H2BmCherry)$^{+}$ cells exhibit clustering (outlined by the white/inner dashed line in C'), whereas the rest (outlined by the yellow/outer dashed line in C') appear unaffected. In these animals, the number of *Tg(neuroD*:GFP)$^{+}$ cells posterior to the PI is significantly increased in comparison to WT animals (quantified in F).

(legend continued on next page)

the direct effects of Notch signaling downregulation on the IPD during feeding stages. Treating WT animals with the γ-secretase inhibitor (GSI) LY411575 [26] from 15–18 dpf increased the β cell number along the IPD (Figures S3O–S3Q), showing that, after Notch signaling downregulation, some IPD cells can differentiate into mature endocrine cells even at these late stages. GSI treatment also caused the clustering of NRCs, as observed in β-cell-ablated animals (Figures S3R and S3S). Altogether, these data suggest that, in β-cell-ablated animals, nutrient intake triggers Notch signaling downregulation in the IPD, leading to progenitor activation. Interestingly, Notch signaling levels were reduced in the IPD of WT animals switched to a high-calorie diet in comparison to those that were maintained on a low-calorie diet between 15–20 dpf (data not shown), indicating that nutrients also modulate Notch signaling under physiological conditions.

Nutrients and TOR Signaling Are Required for the Regenerative Response of the IPD

We classified the phenotypes of β-cell-ablated animals on the basis of the severity of IPD disorganization and the extent of endocrine differentiation (Figures 4A–4F). At 16.5 dpf, 10 out of 34 β-cell-ablated animals (29%) exhibited excessive clustering of the IPD while also having the highest numbers of ectopic endocrine cells (Figures 4D–4F), whereas, at 21.5 dpf, 10 out of 18 animals (56%) exhibited this severe phenotype, suggesting increased penetrance under sustained β cell demand. At 16.5 dpf, we detected rare and weakly insulin$^+$ cells in the PI; however, their numbers did not correlate with the severity of the IPD phenotype. More intriguingly, animals exhibiting the most severe phenotypes were slightly but significantly larger (5.37 ± 0.4 mm, n = 10 animals) in comparison to the rest of the β cell-ablated animals (4.73 ± 0.5 mm, n = 21 animals) ($p < 0.01$). Assuming that growth reflects nutrient intake, these data suggest that higher nutrition in some animals exacerbated the effects of β cell loss. In agreement, dietary restriction, achieved by a 24 hr feeding-fasting regimen from 6–16 dpf, suppressed the IPD phenotypes of β-cell-ablated animals (Figures 4G–4I).

Next, we aimed to identify pathways linking β cell deficiency and nutrient-dependent endocrine differentiation. First, we tested whether increased glucose could stimulate endocrine differentiation. WT larvae were incubated in D-glucose from 3.5–7 dpf, a treatment that increases glucose levels during larval stages [27]. D-glucose treatments increased NRC differentiation into endocrine cells, doubling the number of SIs (Figures S4A, S4B, and S4E). L-glucose, which cannot be utilized as a nutrient, had no effect on endocrine differentiation (n = 28 animals). In addition, glucocorticoid treatment, which increases glucose levels [23], mildly increased SI numbers (Figures S4C–S4E). These data further reveal progenitor sensitivity to nutritional cues, including glucose. Also, we analyzed the role of mTOR, a key intracellular sensor that couples nutrient abundance with cell growth and division across all eukaryotes [28]. To assess its role, we treated β-cell-ablated animals from 8–16 dpf with a low, but effective, dose of the mTOR inhibitor rapamycin (50 nM) [29]. Significantly, this treatment strongly suppressed the β cell ablation phenotypes (Figures 4J–4L). Furthermore, it inhibited the loss of Notch signaling (Figures 4M and 4N), indicating that the activation of IPD cell plasticity in response to nutrient catabolism requires mTOR activity. To analyze mTOR's role in endocrine differentiation under physiological conditions, we counted SIs in WT animals treated with rapamycin or DMSO. Rapamycin treatment significantly reduced the number of newly differentiated SIs, revealing the sensitivity of endocrine progenitors to mTOR activity (Figures 4O–4Q). In addition, PI size was reduced by 26% (2,962 ± 364 μm^2) in comparison to controls (3,985 ± 730 μm^2, n = 10 animals per group, $p < 0.01$), consistent with mTOR's role in endocrine cell growth and proliferation [30, 31]. Importantly, phosphorylated RPS6 (p-RPS6) immunoreactivity, a readout of mTOR activity, was high in the pancreata of fed animals (Figures S4F and S4H) but low after fasting (Figures S4G and S4I), confirming that pancreatic mTOR signaling is responsive to nutrients.

TOR Is Required for Expanding the Progenitor Pool in the IPD

To further assess pancreatic progenitor sensitivity to mTOR activity, we examined their development in a zebrafish mTOR mutant (*mtor*^{xu015Gt}), which develops relatively normally until 7 dpf but exhibits lethality by 10 dpf [32]. In WT animals,

(D) Strong phenotype; complete clustering of the pancreatic NRCs and dramatic increase in *Tg(neuroD*:GFP*)*$^+$ cells (quantified in F).
(E) Distribution of phenotypic classes (no phenotype, 17 animals; moderate phenotype, 7 animals; and strong phenotype, 10 animals).
(F) Quantification of the number of *Tg(neuroD*:GFP*)*$^+$ cells posterior to the PI for each phenotypic class (ns, not significant; *$p < 0.05$, ****$p < 0.0001$).
(G and H) β-cell-ablated animals reared under a normal feeding regimen (G) or a 24 hr feeding-fasting regimen (H) (6–16 dpf).
(I) Distribution of phenotypic classes for control (n = 22) versus dietary restriction (n = 15). The restricted diet suppressed the strong and moderate IPD phenotypes.
(J and K) β-cell-ablated animals treated with DMSO (J) or 50 nM rapamycin (K) (8–16 dpf). The DMSO-treated animals exhibit clustering of the pancreatic NRCs as well as numerous *Tg(neuroD*:GFP*)*$^+$ cells in the pancreatic tail, whereas, in rapamycin-treated animals, the NRCs did not undergo clustering or endocrine differentiation.
(L) Distribution of phenotypic classes for animals treated with DMSO (n = 31) versus rapamycin (n = 16). Rapamycin treatment strongly suppressed the phenotypes observed in β-cell-ablated animals.
(M and N) *Tg(TP1:H2BmCherry); Tg(TP1:VenusPEST)* β-cell-ablated animals treated with DMSO (M) or 50 nM rapamycin (N) (6–16 dpf). Of the ten DMSO-treated animals, three exhibited a loss of *Tg(TP1*:VenusPEST*)* expression in the IPD, whereas, in the rapamycin-treated animals, *Tg(TP1*:VenusPEST*)* expression was maintained (n = 15 animals).
(O and P) WT animals treated with DMSO (O) or 50 nM rapamycin (P) (6–16 dpf). The DMSO-treated animal exhibits five *Tg(neuroD*:GFP*)*$^+$ SIs (arrowheads) in its pancreatic tail, whereas the rapamycin-treated one exhibits two SIs (arrowheads).
(Q) Quantification of the number of SIs posterior to the PI for DMSO- and rapamycin-treated WT animals (n = 28 for DMSO; 27 for rapamycin). Rapamycin reduced the formation of new SIs (***$p < 0.001$). Error bars in (F) = SD, error bars in (Q) = SEM.
(R) Under physiological conditions, high nutrient intake induces β cell proliferation as well as a progressive differentiation of new β cells from the IPD. When the differentiated β cells are ablated, the combination of β cell deficiency and nutrient intake leads to the downregulation of Notch signaling in the IPD. The IPD cells undergo differentiation toward the endocrine lineages as well as an increase in proliferation and loss of ductal characteristics. This process is nutrient dependent, given that it requires high nutrient intake and can be suppressed by a dietary restriction or TOR signaling downregulation.
All panels show lateral views, anterior to the top, dorsal to the left. (M and N) show single planes through the IPD, and all other panels show projections of stacks. Scale bars represent 20 μm.
See also Figure S4.

the pancreatic NRCs proliferate between 2.5–5 dpf and expand posteriorly to form the branched IPD (Figure S4J). In contrast, *mtor*^{xu015Gt} homozygous mutants display a strong defect in NRC expansion, leading to a reduced pool of NRCs and IPD branching defects by 5 dpf (Figure S4K). These data reveal a critical requirement for mTOR in establishing the endocrine progenitor pool during development.

Concluding Remarks

Whereas the effects of glucose on β cell proliferation have previously been described [33–36], we now identify nutrient-sensitive endocrine progenitors in the IPD. Furthermore, we show that β cell deficiency and nutrients cooperate to enhance IPD plasticity and differentiation (Figure 4R). It is likely that, in obesity, impaired β cell function and higher nutrition synergistically regulate progenitor differentiation as well [37]. Indeed, mature pancreatic cell types in mice (including duct cells [38], acinar cells [39], and α cells [40]) exhibit enhanced plasticity after pancreatic injury. We also show that the enhancement of duct cell plasticity in response to β cell loss requires the nutrient sensor mTOR and that Notch signaling, a critical regulator of endocrine differentiation in the embryo [41], is under metabolic control in the mature pancreas. Notably, Notch signaling in human exocrine cells prevents their reprogramming [42]. Furthermore, Notch1 was implicated as a tumor suppressor in a mouse model of pancreatic ductal adenocarcinoma [43], and increased duct cell replication has been reported in type 2 diabetics and obese patients [44], observations consistent with our data in zebrafish. It will be important to identify the metabolic effectors of duct cell plasticity, given that they could provide pharmacological means to enhance β cell differentiation.

Supplemental Information

Supplemental Information contains Supplemental Experimental Procedures and four figures and can be found with this article online at http://dx.doi.org/10.1016/j.cub.2013.05.037.

Acknowledgments

We thank A. Ayala and M. Alva for expert assistance with the fish, O. Stone and A. Villasenor for critical reading of the manuscript, and all members of the Stainier group and A. Schlegel for helpful discussions. We acknowledge the generosity of C. Mosimann for providing *Tg(ubi:Switch)* and technical advice, A. Miyawaki and A. Sakaue-Sawano for providing complementary DNAs encoding (zFucci-S/G2/M) and (zFucci-G1), and X. Xu for *mtor*^{xu015Gt}. This work was supported by postdoctoral fellowships from the Canadian Diabetes Association (N.N.), the Larry L. Hillblom Foundation (D.H.), and the Juvenile Diabetes Research Foundation (D.H.) as well as grants from the National Institutes of Health (R01 DK075032 and U01 DK089541) and the Packard Foundation (D.Y.R.S.). Zebrafish studies were carried out in a designated facility under an International Animal Care and Use Committee license.

Received: December 4, 2012
Revised: March 21, 2013
Accepted: May 21, 2013
Published: June 20, 2013

References

1. Bouwens, L., and Rooman, I. (2005). Regulation of pancreatic beta-cell mass. Physiol. Rev. *85*, 1255–1270.
2. Le Clair, C., Abbi, T., Sandhu, H., and Tappia, P.S. (2009). Impact of maternal undernutrition on diabetes and cardiovascular disease risk in adult offspring. Can. J. Physiol. Pharmacol. *87*, 161–179.
3. Klöppel, G., Löhr, M., Habich, K., Oberholzer, M., and Heitz, P.U. (1985). Islet pathology and the pathogenesis of type 1 and type 2 diabetes mellitus revisited. Surv. Synth. Pathol. Res. *4*, 110–125.
4. Ahrén, J., Ahrén, B., and Wierup, N. (2010). Increased β-cell volume in mice fed a high-fat diet: a dynamic study over 12 months. Islets *2*, 353–356.
5. Maddison, L.A., and Chen, W. (2012). Nutrient excess stimulates β-cell neogenesis in zebrafish. Diabetes *61*, 2517–2524.
6. Kopinke, D., Brailsford, M., Shea, J.E., Leavitt, R., Scaife, C.L., and Murtaugh, L.C. (2011). Lineage tracing reveals the dynamic contribution of Hes1+ cells to the developing and adult pancreas. Development *138*, 431–441.
7. Kopp, J.L., Dubois, C.L., Schaffer, A.E., Hao, E., Shih, H.P., Seymour, P.A., Ma, J., and Sander, M. (2011). Sox9+ ductal cells are multipotent progenitors throughout development but do not produce new endocrine cells in the normal or injured adult pancreas. Development *138*, 653–665.
8. Solar, M., Cardalda, C., Houbracken, I., Martín, M., Maestro, M.A., De Medts, N., Xu, X., Grau, V., Heimberg, H., Bouwens, L., and Ferrer, J. (2009). Pancreatic exocrine duct cells give rise to insulin-producing beta cells during embryogenesis but not after birth. Dev. Cell *17*, 849–860.
9. Ninov, N., Borius, M., and Stainier, D.Y. (2012). Different levels of Notch signaling regulate quiescence, renewal and differentiation in pancreatic endocrine progenitors. Development *139*, 1557–1567.
10. Wang, Y., Rovira, M., Yusuff, S., and Parsons, M.J. (2011). Genetic inducible fate mapping in larval zebrafish reveals origins of adult insulin-producing β-cells. Development *138*, 609–617.
11. Parsons, M.J., Pisharath, H., Yusuff, S., Moore, J.C., Siekmann, A.F., Lawson, N., and Leach, S.D. (2009). Notch-responsive cells initiate the secondary transition in larval zebrafish pancreas. Mech. Dev. *126*, 898–912.
12. Eaton, R.C., and Farley, R.D. (1974). Growth and Reduction of Depensation of Zebrafish, Brachydanio-Rerio, Reared in Laboratory. Copeia, 204–209.
13. Sugiyama, M., Sakaue-Sawano, A., Iimura, T., Fukami, K., Kitaguchi, T., Kawakami, K., Okamoto, H., Higashijima, S., and Miyawaki, A. (2009). Illuminating cell-cycle progression in the developing zebrafish embryo. Proc. Natl. Acad. Sci. USA *106*, 20812–20817.
14. Sakaue-Sawano, A., Kurokawa, H., Morimura, T., Hanyu, A., Hama, H., Osawa, H., Kashiwagi, S., Fukami, K., Miyata, T., Miyoshi, H., et al. (2008). Visualizing spatiotemporal dynamics of multicellular cell-cycle progression. Cell *132*, 487–498.
15. Mosimann, C., Kaufman, C.K., Li, P., Pugach, E.K., Tamplin, O.J., and Zon, L.I. (2011). Ubiquitous transgene expression and Cre-based recombination driven by the ubiquitin promoter in zebrafish. Development *138*, 169–177.
16. Dong, P.D., Munson, C.A., Norton, W., Crosnier, C., Pan, X., Gong, Z., Neumann, C.J., and Stainier, D.Y. (2007). Fgf10 regulates hepatopancreatic ductal system patterning and differentiation. Nat. Genet. *39*, 397–402.
17. Hesselson, D., Anderson, R.M., and Stainier, D.Y. (2011). Suppression of Ptf1a activity induces acinar-to-endocrine conversion. Curr. Biol. *21*, 712–717.
18. Desgraz, R., and Herrera, P.L. (2009). Pancreatic neurogenin 3-expressing cells are unipotent islet precursors. Development *136*, 3567–3574.
19. Deltour, L., Leduque, P., Paldi, A., Ripoche, M.A., Dubois, P., and Jami, J. (1991). Polyclonal origin of pancreatic islets in aggregation mouse chimaeras. Development *112*, 1115–1121.
20. Swenson, E.S., Xanthopoulos, J., Nottoli, T., McGrath, J., Theise, N.D., and Krause, D.S. (2009). Chimeric mice reveal clonal development of pancreatic acini, but not islets. Biochem. Biophys. Res. Commun. *379*, 526–531.
21. Scharfmann, R., Xiao, X., Heimberg, H., Mallet, J., and Ravassard, P. (2008). Beta cells within single human islets originate from multiple progenitors. PLoS ONE *3*, e3559.
22. Herrera, P.L., Huarte, J., Zufferey, R., Nichols, A., Mermillod, B., Philippe, J., Muniesa, P., Sanvito, F., Orci, L., and Vassalli, J.D. (1994). Ablation of islet endocrine cells by targeted expression of hormone-promoter-driven toxigenes. Proc. Natl. Acad. Sci. USA *91*, 12999–13003.
23. Gut, P., Baeza-Raja, B., Andersson, O., Hasenkamp, L., Hsiao, J., Hesselson, D., Akassoglou, K., Verdin, E., Hirschey, M.D., and

Stainier, D.Y. (2013). Whole-organism screening for gluconeogenesis identifies activators of fasting metabolism. Nat. Chem. Biol. *9*, 97–104.

24. Garin, I., Edghill, E.L., Akerman, I., Rubio-Cabezas, O., Rica, I., Locke, J.M., Maestro, M.A., Alshaikh, A., Bundak, R., del Castillo, G., et al.; Neonatal Diabetes International Group. (2010). Recessive mutations in the INS gene result in neonatal diabetes through reduced insulin biosynthesis. Proc. Natl. Acad. Sci. USA *107*, 3105–3110.
25. Wertheimer, E., Lu, S.P., Backeljauw, P.F., Davenport, M.L., and Taylor, S.I. (1993). Homozygous deletion of the human insulin receptor gene results in leprechaunism. Nat. Genet. *5*, 71–73.
26. Fauq, A.H., Simpson, K., Maharvi, G.M., Golde, T., and Das, P. (2007). A multigram chemical synthesis of the gamma-secretase inhibitor LY411575 and its diastereoisomers. Bioorg. Med. Chem. Lett. *17*, 6392–6395.
27. Powers, J.W., Mazilu, J.K., Lin, S., and McCabe, E.R. (2010). The effects of hyperglycemia on adrenal cortex function and steroidogenesis in the zebrafish. Mol. Genet. Metab. *101*, 421–422.
28. Zoncu, R., Efeyan, A., and Sabatini, D.M. (2011). mTOR: from growth signal integration to cancer, diabetes and ageing. Nat. Rev. Mol. Cell Biol. *12*, 21–35.
29. Goldsmith, M.I., Iovine, M.K., O'Reilly-Pol, T., and Johnson, S.L. (2006). A developmental transition in growth control during zebrafish caudal fin development. Dev. Biol. *296*, 450–457.
30. Rachdi, L., Balcazar, N., Osorio-Duque, F., Elghazi, L., Weiss, A., Gould, A., Chang-Chen, K.J., Gambello, M.J., and Bernal-Mizrachi, E. (2008). Disruption of Tsc2 in pancreatic beta cells induces beta cell mass expansion and improved glucose tolerance in a TORC1-dependent manner. Proc. Natl. Acad. Sci. USA *105*, 9250–9255.
31. Balcazar, N., Sathyamurthy, A., Elghazi, L., Gould, A., Weiss, A., Shiojima, I., Walsh, K., and Bernal-Mizrachi, E. (2009). mTORC1 activation regulates beta-cell mass and proliferation by modulation of cyclin D2 synthesis and stability. J. Biol. Chem. *284*, 7832–7842.
32. Ding, Y., Sun, X., Huang, W., Hoage, T., Redfield, M., Kushwaha, S., Sivasubbu, S., Lin, X., Ekker, S., and Xu, X. (2011). Haploinsufficiency of target of rapamycin attenuates cardiomyopathies in adult zebrafish. Circ. Res. *109*, 658–669.
33. Porat, S., Weinberg-Corem, N., Tornovsky-Babaey, S., Schyr-Ben-Haroush, R., Hija, A., Stolovich-Rain, M., Dadon, D., Granot, Z., Ben-Hur, V., White, P., et al. (2011). Control of pancreatic β cell regeneration by glucose metabolism. Cell Metab. *13*, 440–449.
34. Salpeter, S.J., Klein, A.M., Huangfu, D., Grimsby, J., and Dor, Y. (2010). Glucose and aging control the quiescence period that follows pancreatic beta cell replication. Development *137*, 3205–3213.
35. Salpeter, S.J., Klochendler, A., Weinberg-Corem, N., Porat, S., Granot, Z., Shapiro, A.M., Magnuson, M.A., Eden, A., Grimsby, J., Glaser, B., and Dor, Y. (2011). Glucose regulates cyclin D2 expression in quiescent and replicating pancreatic β-cells through glycolysis and calcium channels. Endocrinology *152*, 2589–2598.
36. Dadon, D., Tornovsky-Babaey, S., Furth-Lavi, J., Ben-Zvi, D., Ziv, O., Schyr-Ben-Haroush, R., Stolovich-Rain, M., Hija, A., Porat, S., Granot, Z., et al. (2012). Glucose metabolism: key endogenous regulator of β-cell replication and survival. Diabetes Obes. Metab. *14*(*Suppl 3*), 101–108.
37. Bonner-Weir, S., Toschi, E., Inada, A., Reitz, P., Fonseca, S.Y., Aye, T., and Sharma, A. (2004). The pancreatic ductal epithelium serves as a potential pool of progenitor cells. Pediatr. Diabetes *5*(*Suppl 2*), 16–22.
38. Xu, X., D'Hoker, J., Stangé, G., Bonné, S., De Leu, N., Xiao, X., Van de Casteele, M., Mellitzer, G., Ling, Z., Pipeleers, D., et al. (2008). Beta cells can be generated from endogenous progenitors in injured adult mouse pancreas. Cell *132*, 197–207.
39. Pan, F.C., Bankaitis, E.D., Boyer, D., Xu, X., Van de Casteele, M., Magnuson, M.A., Heimberg, H., and Wright, C.V. (2013). Spatiotemporal patterns of multipotentiality in Ptf1a-expressing cells during pancreas organogenesis and injury-induced facultative restoration. Development *140*, 751–764.
40. Thorel, F., Népote, V., Avril, I., Kohno, K., Desgraz, R., Chera, S., and Herrera, P.L. (2010). Conversion of adult pancreatic alpha-cells to beta-cells after extreme beta-cell loss. Nature *464*, 1149–1154.
41. Apelqvist, A., Li, H., Sommer, L., Beatus, P., Anderson, D.J., Honjo, T., Hrabe de Angelis, M., Lendahl, U., and Edlund, H. (1999). Notch signalling controls pancreatic cell differentiation. Nature *400*, 877–881.
42. Swales, N., Martens, G.A., Bonné, S., Heremans, Y., Borup, R., Van de Casteele, M., Ling, Z., Pipeleers, D., Ravassard, P., Nielsen, F., et al. (2012). Plasticity of adult human pancreatic duct cells by neurogenin3-mediated reprogramming. PLoS ONE *7*, e37055.
43. Hanlon, L., Avila, J.L., Demarest, R.M., Troutman, S., Allen, M., Ratti, F., Rustgi, A.K., Stanger, B.Z., Radtke, F., Adsay, V., et al. (2010). Notch1 functions as a tumor suppressor in a model of K-ras-induced pancreatic ductal adenocarcinoma. Cancer Res. *70*, 4280–4286.
44. Butler, A.E., Galasso, R., Matveyenko, A., Rizza, R.A., Dry, S., and Butler, P.C. (2010). Pancreatic duct replication is increased with obesity and type 2 diabetes in humans. Diabetologia *53*, 21–26.